Polarization response of asymmetric-spiral infrared antennas

C. Fumeaux, G. D. Boreman, W. Herrmann, H. Rothuizen, and F. K. Kneubühl

We present measurements on the polarization response of Ni–NiO–Ni diodes coupled to asymmetric spiral antennas. Our data are for the wavelength dependence of the orientation of the major axis of the polarization ellipse over the wavelength range 10.2–10.7 μm. The data are well fit by a two-wire antenna model. We find that the modes excited on the antenna are a combination of the balanced and unbalanced modes of a two-wire lossy transmission line.

Key words: Spiral antenna, infrared antenna, infrared detector, polarization, metal–oxide–metal diodes.

1. Introduction

Thin-film metal–oxide–metal (MOM) diodes have been developed as fast detectors and mixers of terahertz radiation.[1–3] Diode contact areas as small as 0.012 μm^2 are manufactured[2,3] to achieve a fast temporal response. Various antennas, including dipole[1] and bow-tie[3] configurations, are used for coupling infrared radiation to these small diodes. For this purpose, we investigate spiral antennas, including the relationship of the antenna's geometry and material properties to the measured response of the diode–antenna structure to radiation of various polarization states.

The fabrication of nanometer-scale MOM diodes and antennas has been described elsewhere.[2] The diodes used in this study consist of a NiO layer of 35 Å between two Ni layers of 2200 Å. The two antenna arms are fabricated as two separate depositions of Ni. The metal–oxide layer in the contact region was fabricated after the deposition of the first antenna arm and before the deposition of the second antenna arm. Direct-writing electron-beam lithography[4] was used at the IBM Research Laboratory, Rüschlikon, Switzerland, to define the required patterns. The diode–antenna structure was fabricated on top of a 385-μm-thick silicon substrate. Silicon–dioxide layers of 1.5-μm thickness were used on the top and the bottom of the substrate to improve the coupling efficiency[1] of radiation to the antenna, which receives radiation from the dielectric side more efficiently than from the air.[5] The chip was mounted on a gold socket. Thus infrared radiation from the air side that is transmitted by the substrate is reflected back to the diode and the antenna. Figure 1 is an electron micrograph of the diode and the spiral antenna from the air side; Fig. 2 shows the structure from the substrate side.

Outside the feed region, the logarithmic spiral is defined in polar coordinates $(r; \phi)$ by the general equation[6]:

$$r = r_0 \exp(\phi \ln a) = r_0 a^{\phi}, \tag{1}$$

where r_0 and a are positive constants that determine the radius of the inner structure and the tightness of the spiral. To generate a self-complementary spiral antenna, we used four spirals with relative rotations of $\pi/2$:

$$r_1 = r_0 a^{\phi}, r_2 = r_0 a^{\phi-\pi/2}, r_3 = r_0 a^{\phi-\pi}, r_4 = r_0 a^{\phi+\pi/2}. \tag{2}$$

The antenna consists of metallized areas between spirals 1 and 4 and between spirals 2 and 3, as shown in Fig. 3. Inner and outer diameters are, respectively, $d = 2r_0 = 1.4$ μm and $D = 5.5$ μm. The tightness of the spiral antenna is characterized by a wrap angle β of 80.5°. The antenna feed region is approximated by a combination of elliptical and circular arcs, for the purpose of specifying the electron-

C. Fumeaux, W. Herrmann, and F. K. Kneubühl are with the Institute of Quantum Electronics, Swiss Federal Institute of Technology, CH-8093 Zürich, Switzerland. G. D. Boreman is with the Center for Research and Education in Optics and Lasers (CREOL), University of Central Florida, Orlando, Florida 32816-2700. H. Rothuizen is with the IBM Research Laboratory, Säumerstrasse 4, CH-8803 Rüschlikon, Switzerland.

Received 12 February 1997; revised manuscript received 12 May 1997.

0003-6935/97/256485-06$10.00/0

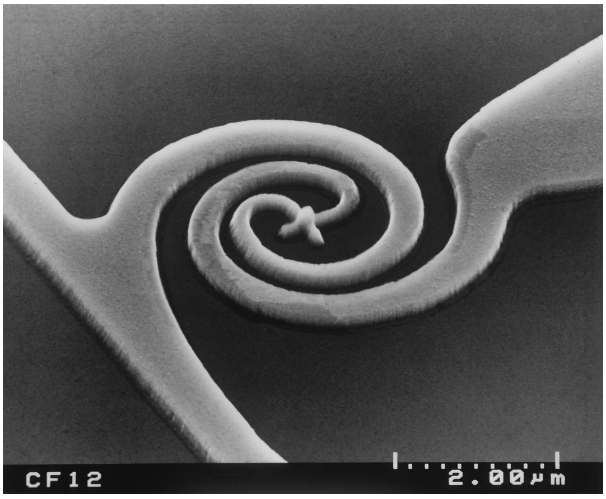

Fig. 1. Electron micrograph of a spiral antenna from the air side.

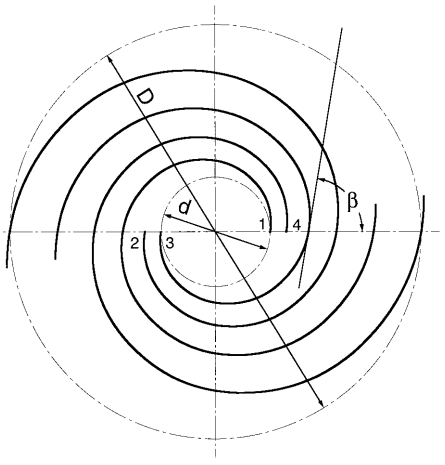

Fig. 3. Spiral structure of antenna outside of feed region.

beam fabrication parameters.[7] Outside the feed region, a combination of decentered quarter-elliptical arcs is an excellent approximation of the desired logarithmic spiral form. The 90° intersection of the antenna arms at the diode was used to relax the tolerance for the relative positions of the two arm depositions. This asymmetric feed region introduces a polarization-dependent antenna responsivity that differs from the circular polarization that would otherwise be expected for a symmetric spiral.

2. Measurement Procedure

The arrangement for the measurement of the polarization dependence of the asymmetric spiral antenna is illustrated in Fig. 4. A grating-tunable flowing-gas CO_2 laser produced linearly polarized infrared radiation in a Gaussian TEM_{00} mode. Tuning the laser over the 10*R* and 10*P* branches of CO_2 permitted generation of wavelengths between 10.2 and 10.7 μm. The experiment was performed in this range because it corresponds to the optimum transmission of the Si/SiO_2 structure.[1] The combination of a CdS 10.6-μm half-wave plate, a 10.6-μm quarter-wave mirror, and a BaF_2 wire-grid polarizer permitted a precise rotation of the linear polarization of the radiation over the wavelength range investigated. The laser beam was chopped at a frequency of 3.6 kHz and focused on the diode with a 12.7-cm focal-length lens. The signal was measured with a lock-in amplifier across a resistor in series with the antenna-coupled diode, while a 160-mV bias was applied to the diode with the arm 2 grounded.

The experiment was performed as follows for each CO_2 laser line investigated: The combination of the half-wave plate and the quarter-wave mirror for 10.6 μm allowed production of nearly circular polarized radiation over the entire wavelength range, by a slight rotation of the fast axis of the half-wave plate with respect to the corresponding position for a 10.6-μm wavelength. We selected any particular linear-polarization component without change of the beam axis by rotating the wire-grid polarizer. The polarizer was mounted on a rotation stage that had an accuracy of approximately 1 arc min. A calibration curve of incident power as a function of polariza-

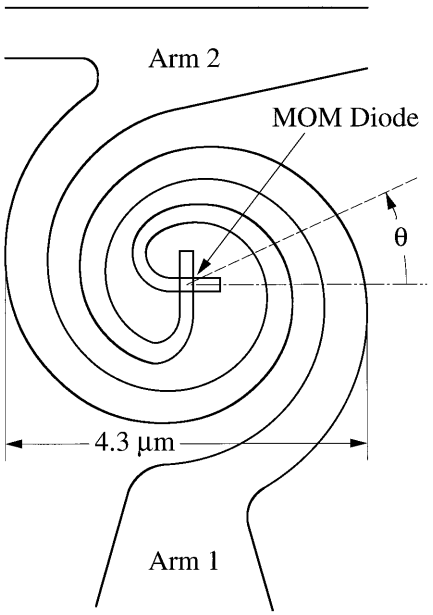

Fig. 2. View of spiral antenna from the substrate side.

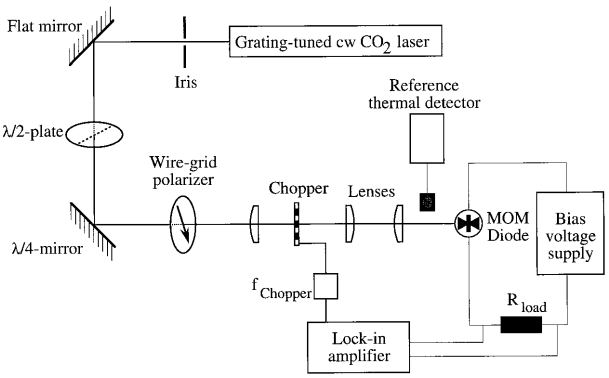

Fig. 4. Experimental apparatus for polarization measurement.

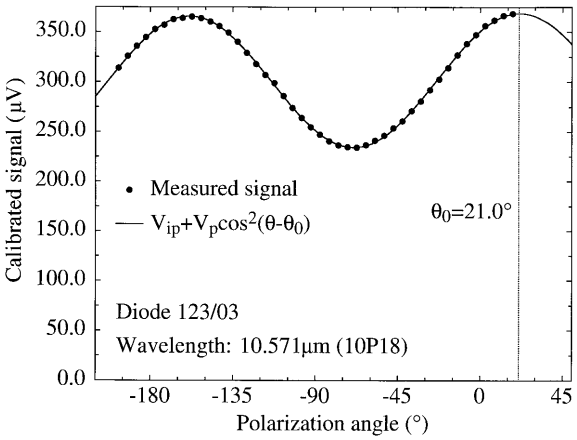

Fig. 5. Polarization dependence of the MOM diode response, allowing determination of θ_0.

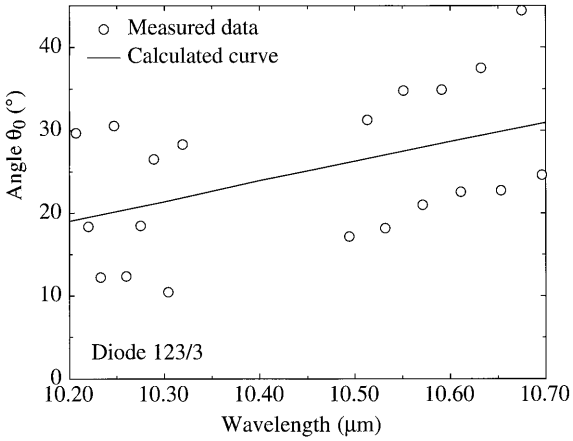

Fig. 6. Wavelength dependence of the orientation θ_0 of the principal axis of the polarization ellipse of the spiral antenna. The solid line is computed from the model.

tion angle θ, as defined in Fig. 2, was measured with a large-area thermal detector. Typical beam power was approximately 100 mW. The laser beam was then focused on the diode at normal incidence. The response of the diode as a function of polarization angle was then measured in 5° increments over a range of ~230°. The measured signal was proportional to the incident laser power for each polarizer setting, so the signal as a function of θ was divided by the calibration curve. The polarization-dependent response was well represented by the sum of a constant and a squared cosine as shown in Fig. 5, which allowed accurate determination of the polarization angle of maximum response. This angle θ_0 corresponds to the orientation of the principal axis of the polarization ellipse of the spiral antenna at the wavelength of the measurement.

3. Measurement Results

The measurement described above was performed for 19 lines of the CO_2 laser spectrum at wavelengths between 10.2 and 10.7 μm. The resulting wavelength dependence of the orientation θ_0 of the major axis of the polarization ellipse of the spiral antenna is presented in Fig. 6. The data show a strong wavelength dependence over the measured range, with fast oscillations superposed. The reproducibility of the data points was within ±1°.

4. Antenna Model

The following model explains the wavelength dependence of the measured θ_0. The current is concentrated near the innermost surface of the spiral antenna.[8] The thin-film spiral antenna is therefore approximated as a thin wire on the inner edge of the metallized part, as shown in Fig. 7. The reciprocity theorem[9] permits the modeling of our antenna as a transmitting antenna and the extension of the results to the actual measured case of a receiving antenna. A traveling wave with the circular frequency ω is sent from the feed point at the diode location and propagates along the antenna as on a lossy transmission line. The infinitesimal current elements on the spiral antenna are assumed to be tangential to the spiral. Their time-dependent amplitude can be described by

$$\delta I = \delta I_0 \cos\left(\frac{2\pi}{\lambda_{\text{eff}}} x - \omega t + \alpha\right)\exp(-\Gamma x), \qquad (3)$$

where x represents the distance from the feed point along the wire, Γ the attenuation, α the phase at the feed point, and λ_{eff} the effective wavelength of the wave propagating on the antenna. In the terahertz range, the effective relative electric permittivity seen by a wave that is propagating on a transmission line approaches the value of the relative electric permittivity $\varepsilon_{\text{subst}} = n^2$ of the substrate.[10] Thus, in terms of

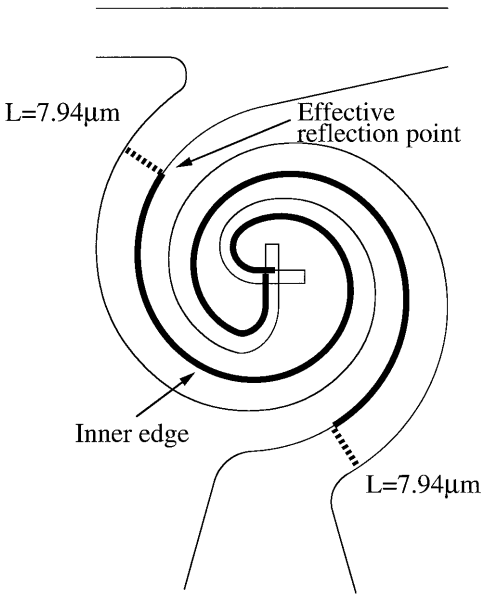

Fig. 7. Wire approximation for current-wave paths used in the model.

the free-space wavelength λ_0, the effective wavelength equals

$$\lambda_{\text{eff}} = \frac{\lambda_0}{\sqrt{\varepsilon_{\text{eff}}}} \approx \frac{\lambda_0}{\sqrt{\varepsilon_{\text{subst}}}} = \frac{\lambda_0}{n}, \tag{4}$$

with $n = 3.45$ for the Si substrate. The attenuation constant measured previously was $\Gamma = 0.15\ \mu\text{m}^{-1}$ for the MOM diodes equipped with dipole antennas.[1] We use the same value of attenuation in our model because of the similarity of materials, fabrication process, and structure dimensions. The vector sum of all the infinitesimal phasor current elements along the spiral wires gives the instantaneous direction and amplitude of the resultant Hertzian dipole. During one period of the 30-THz cycle, this vector rotates by 2π and traces out an ellipse that represents the elliptical polarization state of the antenna. The orientation of the principal axis of this ellipse corresponds to the polarization angle θ_0 of the maximum diode response to linearly polarized radiation.

With regard to the propagating current waves, the antenna is not a balanced structure because of the capacitive impedance of the diode, the asymmetries of the feed structure, and the one-arm-grounded readout configuration. We infer from this imbalance that two current-wave modes will propagate on the structure and thus must be accounted for in the model. The balanced mode has a phase difference of $\Delta\alpha = \pi$ at the feed point between outgoing waves on the two arms of the antenna. The unbalanced mode has a zero interarm phase difference. The effective propagating mode is a linear combination of these two fundamental modes.[11] The mode mixing is described by the unbalanced-mode to balanced-mode amplitude ratio (U/B), which is used as the first fitting parameter in our model.

The spiral antenna forms a transmission line for waves with frequencies of the order of 30 THz. Both the curvature of the antenna structure itself and the terminations of the arms introduce a distributed reflection of the original outgoing wave. In our model we approximate this distributed reflection as a lumped reflection by introducing a discrete location where total reflection of the outgoing wave occurs. The reflected current wave then propagates back toward the feed with a phase shift of π, as required by the boundary condition at the reflection point. The attenuation coefficient used ($0.15\ \mu\text{m}^{-1}$) is such that we neglect a second reflection of the reflected wave at the feed point. The second fitting parameter of our model is accordingly the path length (L) along the wire spiral from the feed to this point of total current-wave reflection.

The following procedure was used to determine the values of the fitting parameters U/B and L. A linear fit to the wavelength-dependent polarization data of Fig. 6 yields $\theta_0 = 30.84°$ for $\lambda_0 = 10.7\ \mu\text{m}$ and a polarization-angle difference of $\Delta\theta_0 = 11.75°$ over the wavelength range 10.2–10.7 μm. Using a summation of outgoing and reflected current waves for both the balanced and the unbalanced modes, we compute

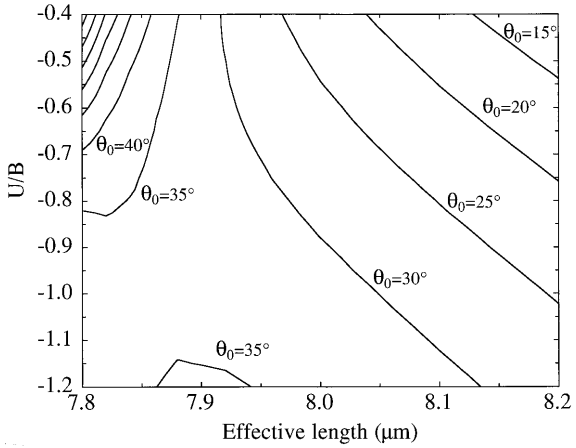

Fig. 8. Computed orientation θ_0 of the principal axis of the polarization ellipse of the spiral antenna at a free-space wavelength of 10.7 μm, as a function of the mode-mixing ratio U/B and the effective arm length before reflection L.

θ_0 at 10.7 μm as a function of U/B and L. The resulting contour plot is shown in Fig. 8. We also compute $\Delta\theta_0$ between 10.2 and 10.7 μm as a function of U/B and L, shown in Fig. 9. The intersection of these two contour plots for the measured values $\theta_0 = 30.84°$ and $\Delta\theta_0 = 11.75°$ yields a simultaneous solution for $U/B = -0.75$ and $L = 7.94\ \mu$m, as shown in Fig. 10. Using these values for U/B and L and our two-mode model, we computed θ_0 *versus* λ_0. The results of this evaluation are shown as the solid line in Fig. 6.

The fast oscillation of the polarization angle θ_0 within the small investigated wavelength range that is apparent in Fig. 6 cannot be explained by this model. A plausible cause may be in the surroundings of the antenna instead of in its structure. The antennas are deposited on a 385-μm-thick silicon substrate covered on both sides with a 1.5-μm-thick SiO_2 layer. This three-layer system is analogous to

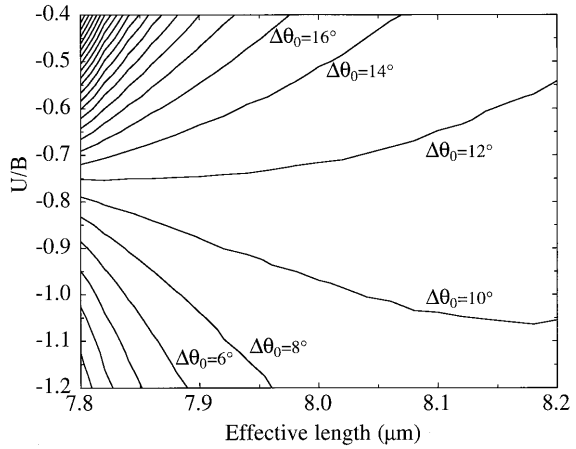

Fig. 9. Computed change $\Delta\theta_0$ in the angle of the principal axis of the polarization ellipse of the spiral antenna over the free-space wavelength range 10.2–10.7 μm, as a function of the mode-mixing ratio U/B and the effective arm length before reflection L.

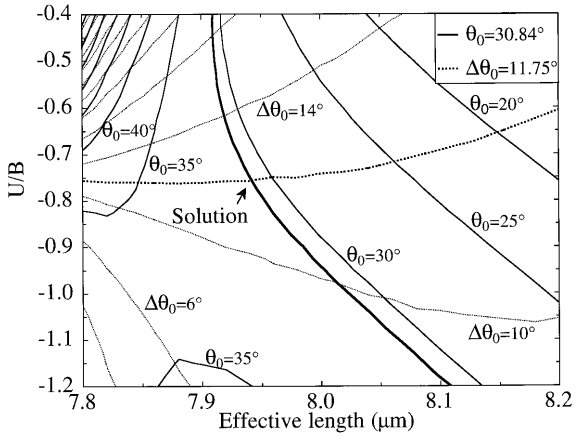

Fig. 10. Intersection of the curves in Figs. 8 and 9 at $U/B = -0.75$ and $L = 7.94$ μm, yielding simultaneous solution for $\theta_0 = 30.84°$ and $\Delta\theta_0 = 11.75°$.

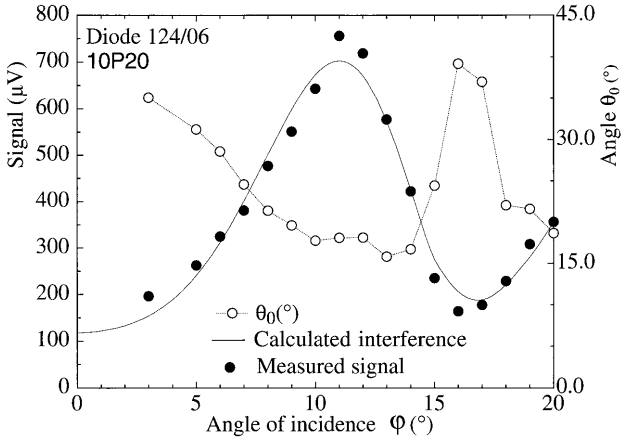

Fig. 12. Measured signal and maximal polarization angle θ_0 *versus* angle of incidence φ.

a Fabry–Pérot interferometer and causes an oscillation of the detected signal magnitudes as the wavelength of the incoming radiation is varied. The antenna is illuminated initially from the air side, while the antenna responsivity is larger for radiation incident from the substrate side. Thus the radiation to which the antenna is most sensitive will be that which has passed through the substrate and is reflected back. This radiation will exhibit strong interference effects that are seen in the response of the antenna as a function of λ_0. An example of detected signals in the 10*P* branch of the CO_2 laser spectrum is shown in Fig. 11. The points indicate measured signal levels, and the dotted curve shows the calculated interference pattern for the substrate. The period of these interferences corresponds to that of the oscillations of θ_0. For the case of constructive interference, the effect of the radiation detected from the air side of the antenna can be neglected. For the case of destructive interference, the small signal levels can be influenced by modes excited by radiation that comes from the air side. The oscillation of the signals that results from these interferences induces an oscillation of the maximum polarization angle θ_0.

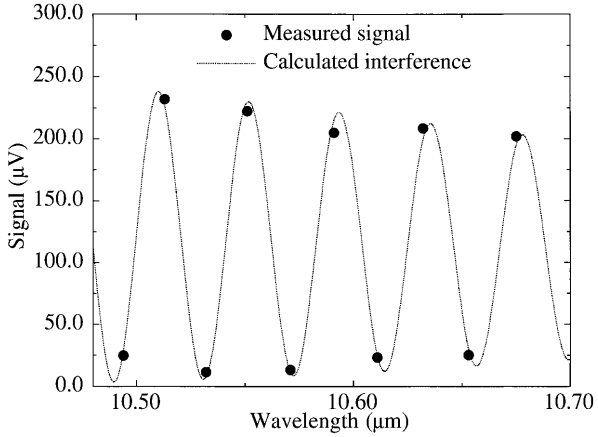

Fig. 11. Oscillation in detected signal *versus* λ_0 caused by substrate interference.

These signal magnitude interference patterns are also detected for a fixed wavelength as the angle of incidence φ is varied. It corresponds that one should also observe oscillations of the angle θ_0 as a function of φ. The scale on the left-hand side of Fig. 12 shows a measurement of the signal as a function of the angle of incidence φ for the 10*P*20 CO_2 laser line at a 10.591-μm wavelength. On the right-hand axis, the same graph also shows the opposing oscillation of the simultaneously measured maximum polarization angle θ_0. The amplitude of these oscillations between $\theta_0 = 15°$ and $\theta_0 = 35°$ corresponds to the measurements shown in Fig. 6 between the 10*P*20 line and the adjacent lines, which confirms that the fast oscillations are caused by a substrate interference effect.

5. Conclusions

In summary, the principal-axis orientation θ_0 of the polarization ellipse of an asymmetric-spiral antenna was measured as a function of wavelength in the 10.2–10.7-μm band. The marked wavelength dependence can be explained by a model based on the vector addition of phasor-current elements tangential to the inner curves of the spiral. We verified that the fast oscillations of θ_0 with wavelength were caused by substrate interference effects.

The current-wave modes that propagated on the antenna arms were a linear combination of a balanced and an unbalanced mode attenuated along the arms and reflected near the arm terminations. The solution for the ratio $U/B = -0.75$ indicates that, in addition to the usual balanced transmission-line mode, a significant unbalanced mode exists on the antenna structure. This imbalance may be caused by the reactive diode impedance, the unbalanced readout configuration, or the asymmetric feed geometry. Reflections of the current waves near the ends of the arms were found to affect the observed polarization behavior for the case investigated where the product of the one-way arm length and the attenuation is of the order of unity. The lumped-reflection model pro-

duced a solution for the effective arm length before reflection of $L = 7.94$ μm, which is somewhat less than the physical length of the antenna arms and indicates the presence of a distributed-reflection mechanism. In our model arm length and phase change on reflection are essentially equivalent quantities so an effective arm length that is shorter than the physical arm length suggests a non-π phase shift on reflection, which would be consistent with a reactive component of the arm-termination impedance.

The authors are indebted to H. Melchior and A. Bohren, Swiss Federal Institute of Technology (ETH) Zürich; P. Vettiger and G. Sasso, IBM Research Laboratory, Rüschlikon; F. Heiniger, Swiss Defense Procurement Agency (GR/EMD), Bern; and I. Wilke, University of Hamburg, for active support and advice. This study was supported by GR/EMD, Bern; Eidgenössische Techniche Hochschule, Zürich; and IBM Research Laboratory, Rüschlikon. G. D. Boreman acknowledges the support of the Ballistic Missile Defense Organization.

References

1. I. Wilke, W. Herrmann, and F. K. Kneubühl, "Integrated nanostrip dipole antennas for coherent 30-THz infrared radiation," Appl. Phys. **B58,** 87–95 (1994).
2. I. Wilke, Y. Oppliger, W. Herrmann, and F. K. Kneubühl, "Nanometer thin-film Ni-NiO-Ni diodes for 30-THz radiation," Appl. Phys. **A58,** 329–341 (1994).
3. C. Fumeaux, W. Herrmann, H. Rothuizen, P. De Natale, and F. K. Kneubühl, "Mixing of 30-THz laser radiation with nanometer thin-film Ni–NiO–Ni diodes and integrated bow-tie antennas," Appl. Phys. **B63,** 135–140 (1996).
4. T. H. P. Chang, D. P. Kern, E. Kratschmer, K. Y. Lee, H. E. Luhn, M. A. McCord, S. A. Rishton, and Y. Vladimirsky, "Nanostructure technology," IBM J. Res. Dev. **32,** 462–493 (1988).
5. C. R. Brewitt-Taylor, D. J. Gunton, and H. D. Rees, "Planar antennas on a dielectric surface," Electron. Lett. **17,** 729–730 (1981).
6. J. D. Dyson, "The equiangular spiral antenna," IRE Trans. Antennas Propag. **7,** 181–187 (1959).
7. F. Vasey, D. Pronguê, H. Rothuizen, and P. Vettiger, "Electron-beam lithography of curved structures with an enhanced vector-scan pattern generator supporting conic-based primitives," J. Vac. Sci. Technol. **B12,** 3460–3464 (1994).
8. G. D. Boreman, A. Dogariu, C. Christodoulou, D. Kotter, "Dipole-on-dielectric model for infrared lithographic spiral antennas," Opt. Lett. **21,** 309–311 (1996).
9. J. R. Carson, "A generalization of the reciprocal theorem," Bell Syst. Tech. J. **3,** 393–399 (1924).
10. W. J. Getsinger, "Microstrip dispersion model," IEEE Trans. Microwave Theory Tech. **MTT-21,** 34–39 (1973).
11. R. G. Corzine and J. A. Mosko, Four-Arm Spiral Antennas (Artech House, Norwood, Mass., 1990).